



# Source apportionment of particulate matter based on numerical simulation during a severe pollution period in Tangshan, North China<sup>☆</sup>

Jianjun He <sup>a, b, \*</sup>, Lei Zhang <sup>a</sup>, Zhanyu Yao <sup>c</sup>, Huizheng Che <sup>a</sup>, Sunling Gong <sup>a</sup>, Min Wang <sup>d</sup>, Mengxue Zhao <sup>d</sup>, Boyu Jing <sup>b</sup>

<sup>a</sup> State Key Laboratory of Severe Weather & Key Laboratory of Atmospheric Chemistry of CMA, Chinese Academy of Meteorological Sciences, Beijing, 100081, PR China

<sup>b</sup> State Environmental Protection Key Laboratory of Odor Pollution Control, Tianjin, 300071, PR China

<sup>c</sup> Key Laboratory of Cloud Physics of CMA & State Key Laboratory of Severe Weather, Chinese Academy of Meteorological Sciences, Beijing, 100081, PR China

<sup>d</sup> Policy Research Center for Environment and Economy, Ministry of Ecology and Environment of the People's Republic of China, Beijing, 100029, PR China

## ARTICLE INFO

### Article history:

Received 26 March 2020

Received in revised form

25 June 2020

Accepted 26 June 2020

Available online 7 July 2020

### Keywords:

Source apportionment

WRF-Chem

FLEXPART

Potential source region

## ABSTRACT

Facing serious air pollution problems, the Chinese government has taken numerous measures to prevent and control air pollution. Understanding the sources of pollutants is crucial to the prevention of air pollution. Using numerical simulation method, this study analysed the contributions of the total local emissions and local emissions from different sectors (such as industrial, traffic, resident, agricultural, and power plant emissions) to PM<sub>2.5</sub> concentration, backward trajectory, and potential source regions in Tangshan, a typical heavy industrial city in north China. The impact of multi-scale meteorological conditions on source apportionment was investigated. From October 2016 to March 2017, total local emissions accounted for 46.0% of the near-surface PM<sub>2.5</sub> concentration. In terms of emissions from different sectors, local industrial emissions which accounted for 23.1% of the near-surface PM<sub>2.5</sub> concentration in Tangshan, were the most important pollutant source. Agricultural emissions were the second most important source, accounting for 10.3% of the near-surface PM<sub>2.5</sub> concentration. The contributions of emissions from power plants, traffic, residential sources were 2.0%, 3.0%, and 7.2%, respectively. The contributions of total local emissions and emissions from different sectors depended on multi-scale meteorological conditions, and static weather significantly enhanced the contribution of regional transport to the near-surface PM<sub>2.5</sub> concentration. Eight cluster backward trajectories were identified for Tangshan. The PM<sub>2.5</sub> concentration for the 8 cluster trajectories significantly differed. The near-surface PM<sub>2.5</sub> in urban Tangshan (receptor point) was mainly from the local emissions, and another important potential source region was Tianjin. The results of the source apportionment suggested the importance of joint prevention and control of air pollution in some areas where cities or industrial regions are densely distributed.

© 2020 Elsevier Ltd. All rights reserved.

## 1. Introduction

With the acceleration of industrialization and urbanization as well as the rapid growth of the number of motor vehicles, air pollution incidents occur frequently in China. From 1980 to 2014, the observed winter haze days in eastern China significantly

increased (Yang et al., 2016). The air quality problems have aroused widespread concern of the government and public. Particle matter with aerodynamic diameter of 2.5 μm or less (PM<sub>2.5</sub>) is the primary pollutant in China, and the Beijing–Tianjin–Hebei region is one of the most polluted areas in China (He et al., 2017b). Although the concentration of PM<sub>2.5</sub> in China has decreased slightly in recent years (Song et al., 2017b), it is much higher than the standard values of the ambient air quality standard (GB 3095-2012) and World Health Organization (Chai et al., 2014). Serious air pollution has adverse effects on human health (An et al., 2015), and a previous study revealed that PM<sub>2.5</sub> pollution contributed as much as 15.5% to all causes of death in 2015 over China (Song et al., 2017a). Since

\* This paper has been recommended for acceptance by Pavlos Kassomenos.

Corresponding author. State Key Laboratory of Severe Weather & Key Laboratory of Atmospheric Chemistry of CMA, Chinese Academy of Meteorological Sciences, Beijing 100081, PR China.

E-mail address: [hejianjun@cma.gov.cn](mailto:hejianjun@cma.gov.cn) (J. He).

2012, a series of air quality standards, control measures, and laws have been promulgated in China. This reflects the tremendous attention of the government to atmospheric environmental issues. Moreover, new requirements and urgent needs have been proposed for the scientific prevention and control of air pollution.

Understanding of the source of air pollution is a key factor for its prevention and control. The methods of source apportionment of PM mainly include the emission inventory method, diffusion model method, receptor model method, and ensemble model method (Shi et al., 2018; Zhang et al., 2015a). The diffusion model method is based on the pollutant emission inventory and meteorological field. The processes of pollutant transport, diffusion, chemical transformation, and deposition in the atmosphere are simulated by a numerical model. The contribution of different pollutant sources to pollutant concentration at the acceptor point is estimated. Based on the Lagrange particle transport diffusion model, the pollutant transport path, backward trajectory, potential source regions, and potential source contribution function are widely investigated (Ding et al., 2013; Dordevic et al., 2019; He et al., 2017c; Liu et al., 2013; Mulder et al., 2019). Based on the Eulerian air quality numerical model, the brute force method, decoupled direct method, adjoint method, tagged species source apportionment method, and Gaussian process emulation method are broadly used for source apportionment (Chen et al., 2020; Dunker et al., 2002; He et al., 2017c; Koo et al., 2009; Wang et al., 2009; Zhai et al., 2018; Zhang et al., 2015b). With linear relationships between concentration and emissions, source apportionment results using different methods are similar or equivalent (Clappier et al., 2017). Source apportionment based on the diffusion model method is not limited to the observation points, and can obtain the spatial distributions of the emission contribution and regional transport. The uncertainties in the diffusion model method originate from the emission inventory, boundary layer meteorological process, and complex atmospheric chemical process (Koo et al., 2009; Zhang et al., 2015a).

Tangshan is located in Hebei province, one of the worst air pollution regions in China (He et al., 2017b). The total resident population is 7.9 million. Tangshan's Gross Domestic Product (GDP) ranked first in Hebei Province, with \$97 billion in 2019 (<https://xw.qq.com/cmsid/20200304A0V6VA00>). Numerous pollution sources, adverse diffusion of the meteorological conditions, and distinct topography are the important reasons for the serious air pollution in the Beijing–Tianjin–Hebei region (Gao et al., 2011; He et al., 2017a; Zhang et al., 2018). According to “Brief Situation of National Eco-environmental Quality in 2018”, Tangshan ranked fourth in the cities with poor air quality in China in 2018 (<https://baijiahao.baidu.com/s?id=1628312479084586136&wfr=spider&for=pc>). Sulfur dioxide and nitrogen oxides emissions in Tangshan reached  $159 \times 10^3$  and  $204 \times 10^3$  tons in 2017 (<http://www.tangshan.gov.cn/zhuzhan/tjxxnb/20190115/669214.html>). Numerous studies on the causes of air pollution focus on large cities, such as Beijing, Tianjin, and Shijiazhuang. There is little research investigating the sources of the atmospheric pollutants and influences of the meteorological conditions over Tangshan. Using the Weather Research and Forecasting model coupled to Chemistry (WRF-Chem) and FLEXible PARTicle (FLEXPART) dispersion model, this study analyses the contributions of the local emissions on PM<sub>2.5</sub> concentration, backward trajectory, and potential source regions in Tangshan. The impact of atmospheric circulation on the source apportionment is studied. The results are of tremendous significance for understanding the causes of air pollution and adopting air pollution prevention and control measures in Tangshan and similar cities.

## 2. Data and methods

### 2.1. WRF-Chem simulation setting

WRF-Chem is an online coupled air quality numerical model. It was developed and supported by the National Oceanic and Atmospheric Administration (NOAA), National Center for Atmospheric Research (NCAR) and other organizations or institutions. WRF-Chem V3.9 is used to investigate the contribution of total local emissions and emissions of different sectors to the near-surface PM<sub>2.5</sub> concentration.

WRF-Chem is configured to have two nested domains with horizontal resolutions of 25 km ( $140 \times 100$  girds) covering most part of eastern China, and 5 km ( $100 \times 100$  girds) covering Tangshan and surrounding cities (Fig. 1a). In the vertical direction, there are 35 vertical levels extending from the surface to 50 hPa, with 12 levels in the lowest 1 km. The meteorological initial and lateral boundary conditions are provided by the FNL (Final) Operational Global Analysis data (<https://rda.ucar.edu/datasets/ds083.2/>). Chemical initial fields use default idealized profile obtained from WRF-Chem. The time steps of the two nested domains are 150 s and 30 s, respectively. The output time interval of WRF-Chem is 1 h. The period of simulation is from October 2016 to March 2017, a serious pollution period for north China. The simulation is integrated once a month. To decrease the impact of the chemical initial fields, ten extra days for each run are simulated as the spin-up time and are not included in the follow-up analysis. Analysis nudging is used to constrain the simulated meteorological fields from WRF to derive the field (Carvalho et al., 2012).

The uncertainty in an emission inventory is an important reason causing the error in air quality simulations (Saikawa et al., 2017). In this study, the Multi-resolution Emission Inventory for China (MEIC) at 0.25° in 2016 is used. MEIC has five source sectors, i.e. industries emissions, power plant emissions, traffic emissions, resident emissions, and resident emissions (<http://www.meicmodel.org/>). The spatial distribution of the PM<sub>2.5</sub> emission is shown in Fig. 1 (c). The Tangshan urban area is the most important pollution source in the study area.

Meteorological parameterization schemes include the single-moment 6-class microphysics scheme (Hong and Lim, 2006), Kain–Fritsch cumulus scheme for the outer domain (Kain, 2004), rapid radiative transfer model for the longwave radiation scheme (Mlawer et al., 1997), Dudhia shortwave radiation scheme (Dudhia, 1989), Yonsei University (YSU) planetary boundary layer scheme (Hong et al., 2006), and Noah land surface model scheme (Chen and Dudhia, 2001). These parameterization schemes have been widely used and evaluated in previous studies (He et al., 2017d). For gas-phase chemicals, the second-generation regional acid deposition model (RADM2) chemical mechanism is used (Stockwell et al., 1990). For aerosol chemistry, the modal aerosol dynamics model for Europe/secondary organic aerosol model (MADE/SORGAM) mechanism is adopted (Schell et al., 2001). Aerosol chemical components of MADE/SORGAM include sulphate ( $\text{SO}_4^{2-}$ ), nitrate ( $\text{NO}_3^-$ ), ammonium ( $\text{NH}_4^+$ ), sodium ion ( $\text{Na}^+$ ), chloride ion ( $\text{Cl}^-$ ), dust aerosol, elemental carbon (EC), primary organic aerosol (POA), and secondary organic aerosol (SOA). Previous studies revealed that WRF-Chem with RADM2- MADE/SORGAM has a good performance in aerosol optical depth (AOD) simulation (Balzarini et al., 2015). In addition, Madronich photolysis is selected.

Reviewing widely used source apportionment methods for air quality management, the brute force method are the best suited to

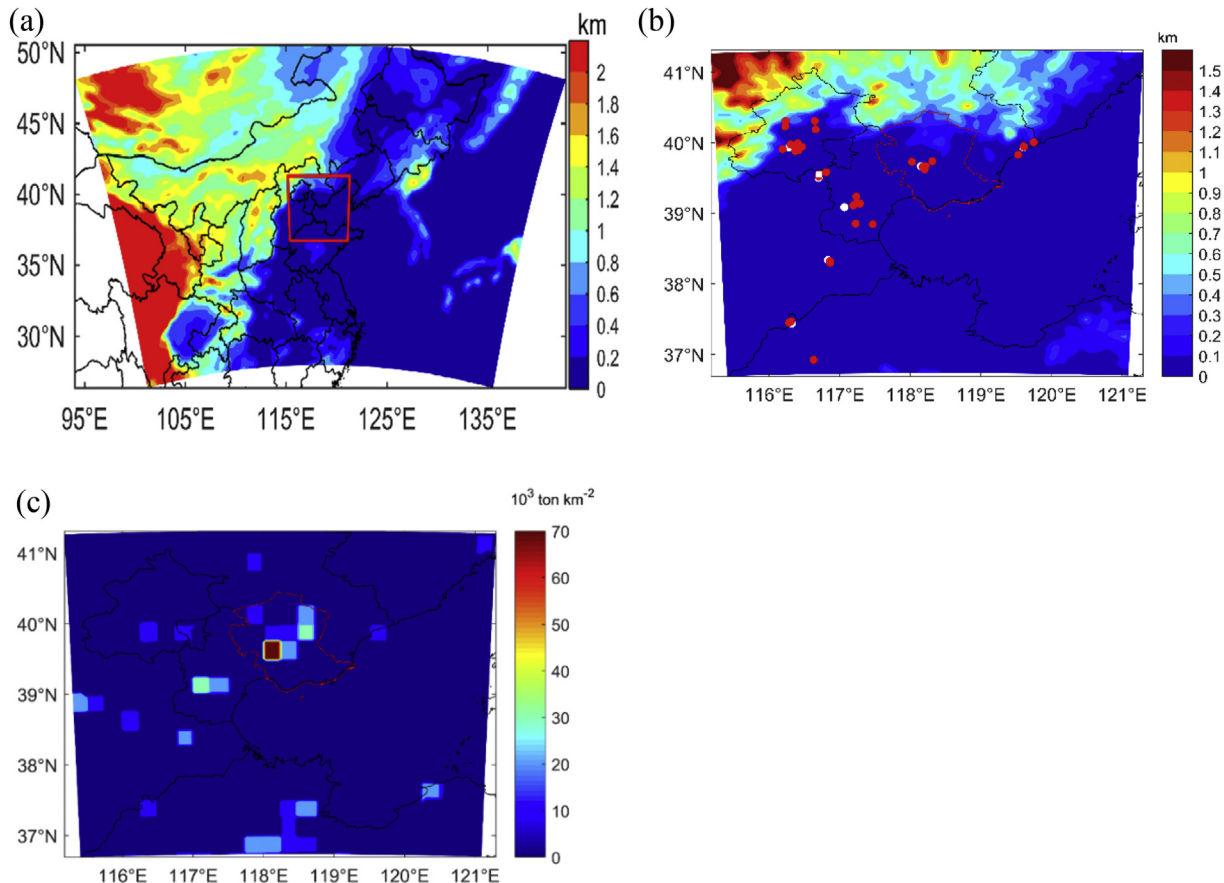


**Fig. 1.** Two nested domains for WRF-Chem with horizontal resolutions of 25 km and 5 km (a), observation station distribution (red points represent air quality stations, white square represents chemical composition observation station, and white points represent meteorological stations) in the inner domain (b), and spatial distribution of the PM<sub>2.5</sub> emission in the inner domain (c). The black line represents the boundaries of the provinces, and the red line in (b) and (c) represents the boundary of Tangshan. (For interpretation of the references to colour in this figure legend, the reader is referred to the Web version of this article.)

support air quality planning (Thunis et al., 2019). The brute force method (emission switch on/off method) is used to investigate the contributions of the different source emissions to the PM<sub>2.5</sub> concentration. The base simulation (BASE) uses the normal MEIC inventory and is evaluated by comparison with meteorological and air quality observation data. Six sensitivity simulations (SEN) are conducted using the MEIC inventory, removing Tangshan's total local emissions, local industries emissions, local power plant emissions, local traffic emissions, local resident emissions, and local agricultural emissions. The contributions of the total local emissions (LOC), local industrial emissions (IND), local power plant emissions (POW), local traffic emissions (TRA), local resident emissions (RES), and local agricultural emissions (AGR) to the near-surface PM<sub>2.5</sub> concentration are calculated by comparison with the base simulation and sensitivity simulations.

## 2.2. FLEXPART simulation setting

The FLEXible PARTICle (FLEXPART) dispersion model is an off-line Lagrangian particle transport and diffusion model developed by the Norwegian Institute of Air Research. By calculating the transport and diffusion processes of the particles released from point, line, surface, or volume sources in the atmosphere, FLEXPART can be used to study the pollutant long-distance and mesoscale transport, diffusion, wet and dry deposition, radiation attenuation and other processes in the atmosphere. Forward integration can simulate the diffusion process of the pollutants, and backward

integration can be used to simulate the contributions of the potential sources.

WRF supplies the meteorological fields to drive FLEXPART. The time step of FLEXPART is 180 s, and the output time interval is 1 h. It is worth to point out that the uncertainty in the Lagrange trajectory simulation can be reduced by using the average wind field (Brioude et al., 2013). FLEXPART is driven by the average wind field of WRF, and the time deviation caused by the average wind field is corrected by the time correction option. The CBL turbulence parameterization scheme is used to simulate the contribution of the air mass. For backward trajectory simulation, CBL turbulence parameterization is switched off. The parameters of the boundary layer and near-surface are obtained from the WRF simulation. It is sufficient using 24 h backward trajectory to determine probable locations of regional emission sources and explain regional transport pathways for North China (Wang et al., 2010). Hence, the particle residence time is set as 24 h. The setting of FLEXPART is the same as in previous studies (He et al., 2017c). Increasing the number of released particles will lead to an increase in the computing resources. Considering turbulent diffusion and computing resources, the release point (acceptor point) is determined to release 200 tracer particles per hour.

Because the most anthropogenic emission sources are located below 100 m, the source of the air mass from the surface to 100 m layer is used to investigate the potential source of PM<sub>2.5</sub>. The contribution of the primary PM<sub>2.5</sub> sources ( $CR_{PM2.5}$ ) used to describe the potential source of PM<sub>2.5</sub>, considers the contribution of the air

mass ( $CR_{air}$ ) and PM<sub>2.5</sub> emission ( $E_{PM_{2.5}}$ ) synthetically, as calculated in Eq. (1) (He et al., 2017c). The contribution of the air mass is the ratio of tracer particles in a grid to total tracer particles released from receptor point.

$$CR_{PM_{2.5}} = CR_{air} \times E_{PM_{2.5}} \times 100\% \quad (1)$$

### 2.3. Objective circulation classification

Meteorological conditions are important factors affecting the pollutant concentration, pollutant transport and dispersion, and source–sink process of air pollution (He et al., 2017b; He et al., 2017c). In this study, the impact of the circulation type on source apportionment is investigated. Based on the European Centre for Medium-Range Weather Forecasts (ECMWF) ERA-Interim sea level pressure (SLP) reanalysis data at 08:00 (Beijing Time) from October 2016 to March 2017, the T-mode principal component analysis (PCA) combined with the K-means cluster is used to identify the circulation type. First, three-dimensional ERA SLP grid data (longitude × latitude × time) was reshaped to two-dimensional data (grid × time). Second, the reshaped SLP data was normalized using z-scores method for time series. Third, the normalized data performed PCA. Then the main components were obtained according to the cumulative variance contribution of 85%. Finally, the main components were clustered using the K-means cluster, and synoptic-scale circulations were ascertained based on cluster results.

Fig. 2 shows the mean sea-level pressure and occurrence frequencies of eight circulation types (CT). The different circulation types have different atmospheric diffusion capabilities and pollutant concentration levels. For CT1, the uniform pressure field results in a low wind speed and poor diffusion conditions. For CT2 and CT4, Tangshan is located in the low-pressure area. A northeast–southwest convergence zone is formed, which is not conducive to pollutant diffusion. For CT3, Tangshan is located at the back of the high pressure. According to geostrophic wind theory, the Beijing–Tianjin–Hebei region is controlled by the southwest wind. It easily leads to formation of the regional transport of the pollutants and causes serious pollution in Tangshan. Under the influence of cold air in autumn and winter in North China, the pressure gradient and wind force usually increase. CT5, CT6, and CT7 represent cold air processes with different intensities, which are beneficial for pollutant dispersion. CT8 is a typical stable weather, and Tangshan is situated in the centre of a high-pressure region. The development of the boundary layer and diffusion of pollutants are inhibited by the subsidence airflow in the high-pressure zone.

### 2.4. Meteorological and air quality observation data

Daily near-surface meteorological observations, including 2-m temperature ( $T_2$ ), 2-m relative humidity ( $RH_2$ ), and 10-m wind speed ( $WS_{10}$ ), from Oct. 2016 to Mar. 2017, are provided by the National Meteorological Information Centre (NMIC) to evaluate the performance of WRF. The locations of seven meteorological observatories, i.e., Beijing, Tianjin, Tangshan, Qinhuangdao, Langfang, Cangzhou, and Dezhou, are shown in Fig. 1b. Hourly six pollutant concentrations, i.e., PM<sub>2.5</sub>, particle matter with aerodynamic diameter of 10 μm or less (PM<sub>10</sub>), sulfur dioxide (SO<sub>2</sub>), nitrogen dioxide (NO<sub>2</sub>), carbon monoxide (CO), ozone (O<sub>3</sub>), from Oct. 2016 to Mar. 2017, are acquired from China National Environmental Monitoring Centre (CNEMC) to evaluate the performance of WRF-Chem. The details of air quality instruments and data quality control can

be referred to previous study (Zhao et al., 2016). In addition to conventional air quality observations, chemical component observations at Langfang during Mar. 2017 are also used to assess the ability of simulating chemical components. Water soluble ions, including SO<sub>4</sub><sup>2-</sup>, NO<sub>3</sub><sup>-</sup>, NH<sub>4</sub><sup>+</sup>, etc., are observed by water soluble ion on-line analyser (WAGA-100). EC and organic carbon (OC) are observed by atmospheric OC/EC on-line analyser. It is difficult to distinguish POA and SOA from observed OC. So the simulated POA and SOA are added and compared with the observed OC. The locations of air quality observatories are shown in Fig. 1b.

### 2.5. Model evaluation method

Five statistical indices, i.e., index of agreement (IOA), correlation coefficient (R), root mean square error (RMSE), mean bias (MB) and mean error (ME), are used for model evaluation, as shown in Eqs. (2)–(6):

$$IOA = 1 - \sum_{i=1}^N (F_i - O_i)^2 \left/ \sum_{i=1}^N (|F_i - \bar{O}| + |O_i - \bar{O}|)^2 \right. \quad (2)$$

$$R = \frac{1}{N} \sum_{i=1}^N (F_i - \bar{F}) \times (O_i - \bar{O}) \left/ \left[ \sqrt{\frac{1}{N} \sum_{i=1}^N (F_i - \bar{F})^2} \sqrt{\frac{1}{N} \sum_{i=1}^N (O_i - \bar{O})^2} \right] \right. \quad (3)$$

$$RMSE = \sqrt{\frac{1}{N} \sum_{i=1}^N (F_i - O_i)^2} \quad (4)$$

$$MB = \frac{1}{N} \sum_{i=1}^N |F_i - O_i| \quad (5)$$

$$ME = \frac{1}{N} \sum_{i=1}^N |F_i - O_i| \quad (6)$$

where  $F$  and  $O$  are the simulated and the observed values, respectively,  $\bar{F}$  and  $\bar{O}$  are the mean simulated and observed values, respectively, and  $N$  is the number of samples.

## 3. Results and discussions

### 3.1. Model evaluation

The good performance of the meteorological simulation is an important basis for pollutant diffusion simulation by FLEXPART and air quality simulation by WRF-Chem. The statistical performances of  $T_2$ ,  $RH_2$ , and  $WS_{10}$  are listed in Table 1. WRF underestimates  $T_2$  and  $RH_2$  with an MB of  $-1.97\text{ K}$  and  $-5.21\%$  and overestimates  $WS_{10}$  with an MB of  $0.68\text{ m s}^{-1}$ . The IOA and R for  $T_2$  are 0.95 and 0.94, respectively, whereas they are 0.84 and 0.73 for  $RH_2$ . This suggests that WRF well reproduces the change characteristics of  $T_2$  and  $RH_2$ . The performance of  $WS_{10}$  is also good because the IOA and RMSE meet the statistical benchmarks ( $\geq 0.6$  and  $\leq 2$ ) for wind speed (He et al., 2014). The statistical performance of the near-surface meteorology is also comparable to previous studies (Carvalho et al., 2012; He et al., 2017d). Generally, WRF well reproduces the temporal–spatial change characteristics of the meteorological fields in the inner domain.

Fig. 3 shows the comparison of the observed and simulated daily

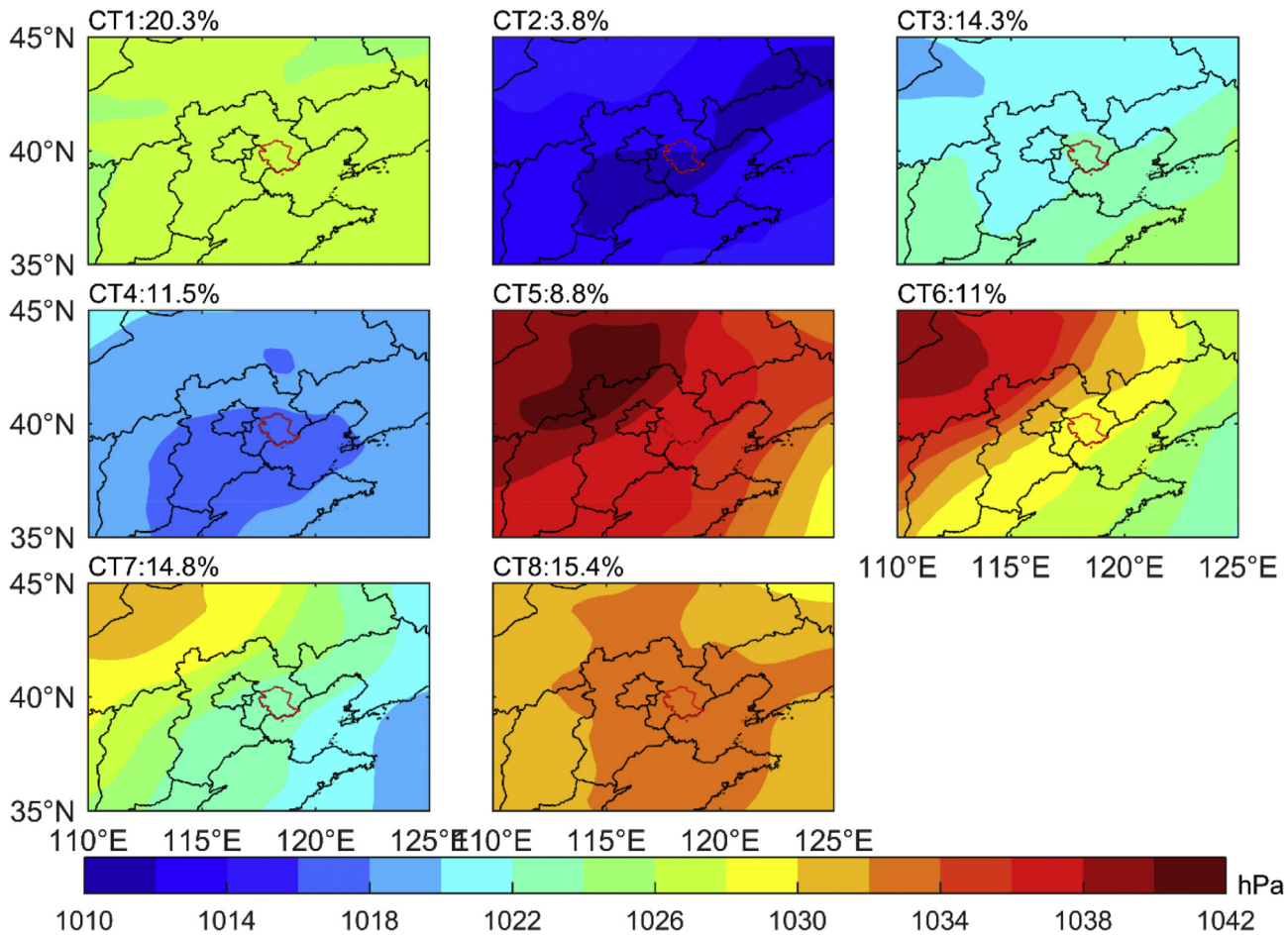


**Fig. 2.** Mean sea-level pressures and occurrence frequencies of eight circulation types. The colour bar represents the mean sea-level pressure, black line represents the boundaries of the province, and the red line represents the boundary of Tangshan. (For interpretation of the references to colour in this figure legend, the reader is referred to the Web version of this article.)

**Table 1**  
Statistical performances of the daily near-surface meteorological conditions and pollutant concentrations.

	IOA	R	RMSE	MB	ME
T <sub>2</sub>	0.95	0.94	2.93 (K)	-1.97 (K)	2.36 (K)
RH <sub>2</sub>	0.84	0.73	15.63 (%)	-5.21 (%)	12.37 (%)
WS <sub>10</sub>	0.62	0.49	1.21 (m s <sup>-1</sup> )	0.68 (m s <sup>-1</sup> )	0.94 (m s <sup>-1</sup> )
PM <sub>2.5</sub>	0.85	0.85	39.2 ( $\mu\text{g m}^{-3}$ )	-21.2 ( $\mu\text{g m}^{-3}$ )	26.9 ( $\mu\text{g m}^{-3}$ )
PM <sub>10</sub>	0.69	0.81	77.0 ( $\mu\text{g m}^{-3}$ )	-40.3 ( $\mu\text{g m}^{-3}$ )	61.1 ( $\mu\text{g m}^{-3}$ )
SO <sub>2</sub>	0.85	0.79	10.9 ( $\mu\text{g m}^{-3}$ )	5.3 ( $\mu\text{g m}^{-3}$ )	8.0 ( $\mu\text{g m}^{-3}$ )
NO <sub>2</sub>	0.79	0.83	17.3 ( $\mu\text{g m}^{-3}$ )	-13.4 ( $\mu\text{g m}^{-3}$ )	14.5 ( $\mu\text{g m}^{-3}$ )
CO	0.59	0.79	1.1 ( $\text{mg m}^{-3}$ )	-0.8 ( $\text{mg m}^{-3}$ )	0.8 ( $\text{mg m}^{-3}$ )
O <sub>3</sub>	0.62	0.61	15.3 ( $\mu\text{g m}^{-3}$ )	0.4 ( $\mu\text{g m}^{-3}$ )	13.0 ( $\mu\text{g m}^{-3}$ )

average PM<sub>2.5</sub> concentration. WRF-Chem performs well in the daily variation in the PM<sub>2.5</sub> concentration. WRF-Chem can well reproduce daily variation of PM<sub>2.5</sub> concentration. WRF-Chem underestimates the PM<sub>2.5</sub> concentration in the serious pollution period, whereas it well reproduces the PM<sub>2.5</sub> concentration on a normal and clean day. The statistical performance of six pollutant concentrations (Table 1) could give more comprehensive understanding on the capability of WRF-Chem. The high R of simulated and observed regional average pollutant concentrations imply good performance in temporal variation of pollutant concentrations. Compared to other pollutants, the formation of O<sub>3</sub> is more complex, leading to relative low values of IOA and R. The simulated PM<sub>2.5</sub>,

PM<sub>10</sub>, NO<sub>2</sub>, and CO concentrations are 21.2  $\mu\text{g m}^{-3}$ , 60.3  $\mu\text{g m}^{-3}$ , 13.4  $\mu\text{g m}^{-3}$ , and 0.78 mg  $\text{m}^{-3}$  lower than the observed average concentration. While the simulated SO<sub>2</sub> and O<sub>3</sub> concentrations are slightly higher than the observed average concentrations. Generally, the statistical indices are comparable to or even better than the results of similar simulation studies (Gao et al., 2011).

Besides the PM<sub>2.5</sub> mass concentration, the performance of a chemical component in PM<sub>2.5</sub> is an important indicator for the accuracy of the chemical species in the emission inventory and aerosol and gas chemical mechanisms. Fig. 4 shows the observed and forecasted SO<sub>4</sub><sup>2-</sup>, NO<sub>3</sub><sup>-</sup>, NH<sub>4</sub><sup>+</sup>, EC, and OC concentrations in Langfang during Mar. 2017. Observed SO<sub>4</sub><sup>2-</sup>, NO<sub>3</sub><sup>-</sup>, NH<sub>4</sub><sup>+</sup>, EC, and OC average concentrations are 15.3  $\mu\text{g m}^{-3}$ , 10.1  $\mu\text{g m}^{-3}$ , 7.7  $\mu\text{g m}^{-3}$ , 2.2  $\mu\text{g m}^{-3}$ , and 13.2  $\mu\text{g m}^{-3}$ , respectively. WRF-Chem underestimates SO<sub>4</sub><sup>2-</sup>, NH<sub>4</sub><sup>+</sup>, EC, and OC concentrations, while overestimates NO<sub>3</sub><sup>-</sup> concentration. Fortunately, WRF-Chem can well reproduce temporal change of chemical components, with the Rs of 0.72, 0.55, 0.7, 0.73 and 0.71 for hourly O<sub>4</sub><sup>2-</sup>, NO<sub>3</sub><sup>-</sup>, NH<sub>4</sub><sup>+</sup>, EC, and OC concentrations (Table 2). Previous studies revealed that NO<sub>x</sub> from vehicles is one important source of the precursors of particulate nitrate over North China Plain (He et al., 2016; Wang et al., 2020). The contribution of NO<sub>3</sub><sup>-</sup> is high, which may be related to the increase in vehicles in recent years. In recent year, the SO<sub>2</sub> emission and SO<sub>2</sub> concentration have significantly decreased in China (He et al., 2017b; He et al., 2018). However, SO<sub>4</sub><sup>2-</sup> is still a very important chemical component of PM<sub>2.5</sub>. The significant underestimation

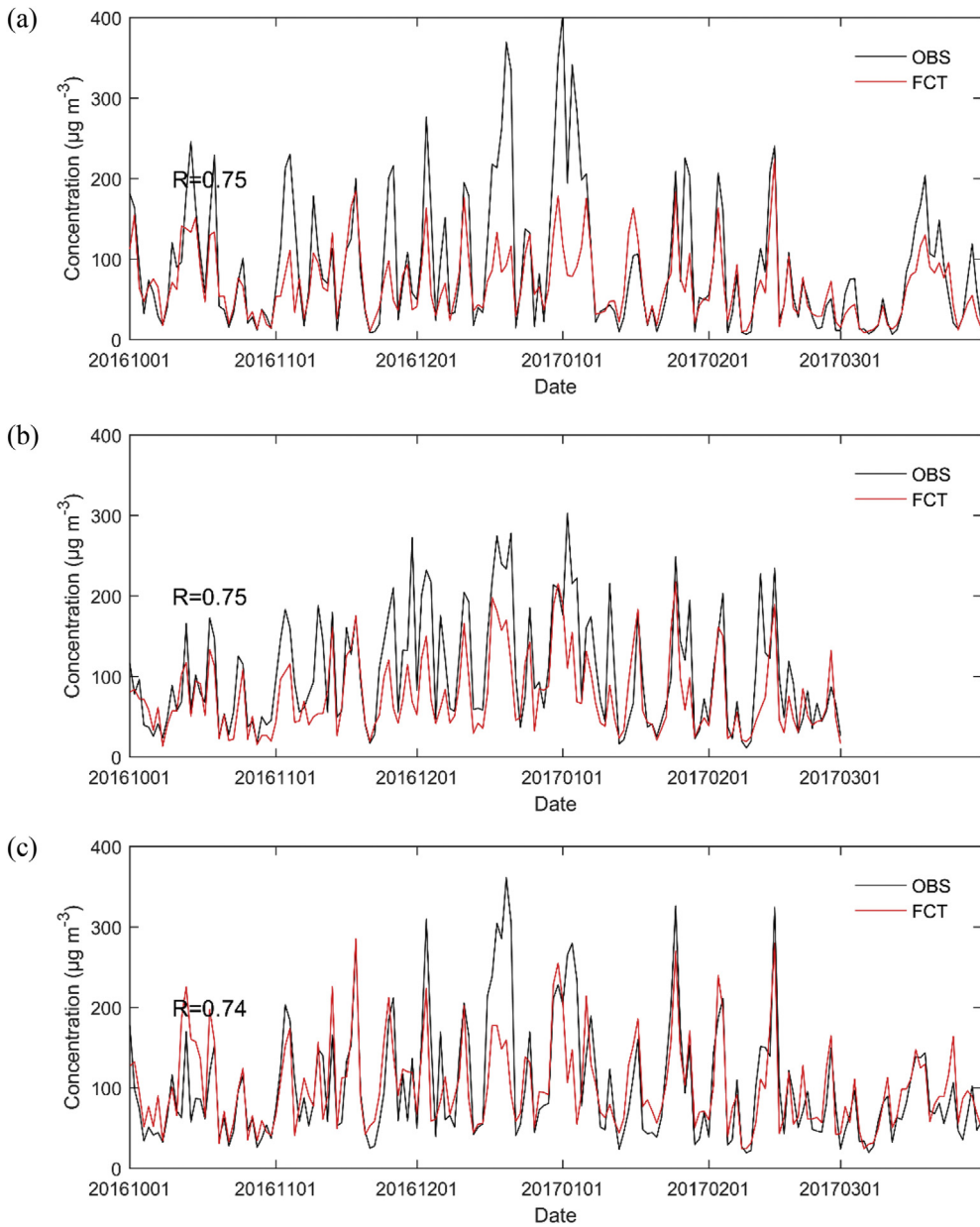


**Fig. 3.** Comparison of the observed (OBS) and forecasted (FCT) near-surface  $\text{PM}_{2.5}$  daily mean concentrations in Beijing (a), Tianjin (b), and Tangshan (c).

of  $\text{SO}_4^{2-}$  concentration is also found in other studies, which may be related to the incomplete atmospheric chemical processes (such as heterogeneous chemical process) in WRF-Chem (Gao et al., 2016). However, significant uncertainty of the uptake coefficient results in large uncertainty of heterogeneous chemical process and hinders the application of heterogeneous chemical processes in atmospheric chemical model (Zheng et al., 2015). The underestimation of  $\text{SO}_4^{2-}$  and OC in heavy pollution results in the underestimation of  $\text{PM}_{2.5}$  concentration peak (Fig. 3). Except  $\text{SO}_4^{2-}$ , the contributions of the chemical components from WRF-Chem seem reasonable.

### 3.2. Contribution of different emission sources

The contributions of the different emission sources to the near-surface  $\text{PM}_{2.5}$  concentration are obtained by the emission switch on/off method. However, the brute force method may change the oxidation capacity of the air and thus will give inconsistent results.

Based on the results of the brute force method, daily contribution of IND, POW, TRA, RES, AGR, and LOC to the near-surface  $\text{NO}_3^-$  concentration in Tangshan is analysed (Fig. 5). The  $\text{NO}_3^-$  concentration from LOC is basically the same as the sum of  $\text{NO}_3^-$  concentration from different emission sources. Similar phenomenon is found for  $\text{SO}_4^{2-}$ ,  $\text{NH}_4^+$ , and SOA, indicating that the brute force method is suitable for source apportionment in Tangshan.

The contribution of LOC to the near-surface  $\text{PM}_{2.5}$  concentration is 46.0%. Although the total emission in the Tangshan urban area is higher than that in the surrounding urban area (Fig. 1c), more than half of  $\text{PM}_{2.5}$  is from the trans-boundary contribution. A significant regional transport indicates that the air pollution in the Beijing–Tianjin–Hebei region presents regional pollution characteristics, and the government should conduct a joint prevention and control of the regional pollution. IND is the most important pollution source in Tangshan, and contributes more than 60% of the pollutant emissions, except ammonia ( $\text{NH}_3$ ) (Table 3). However, the

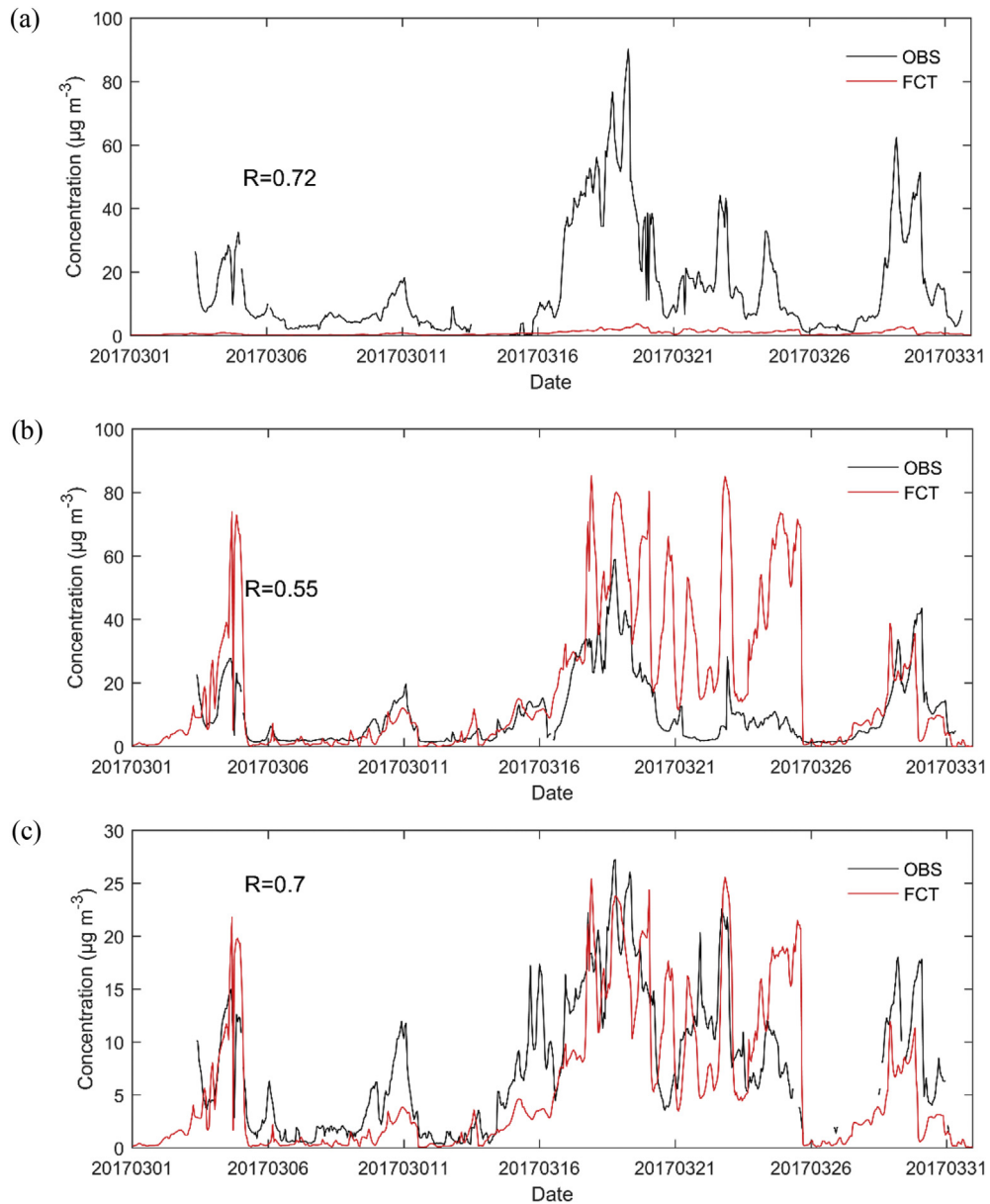


**Fig. 4.** Comparison of the observed (OBS) and forecasted (FCT)  $\text{SO}_4^{2-}$  (a),  $\text{NO}_3^-$  (b),  $\text{NH}_4^+$  (c), EC (d), and OC (e) concentrations in Langfang during Mar. 2017.

contribution of IND to the near-surface PM<sub>2.5</sub> concentration is 23.1%, and 50.2% for the PM<sub>2.5</sub> formed by the total local emissions. The contribution of IND to the PM<sub>2.5</sub> concentration is obviously lower than the contribution of the IND emission to the total emissions. A similar phenomenon is found for POW, whose contributions to the near-surface PM<sub>2.5</sub> concentration and PM<sub>2.5</sub> formed by the local emission are 2.0% and 4.4%, respectively, which are lower than the contribution of the POW emission in the total emission. This may be related to the following two reasons. First, more secondary aerosols, such as ammonium and nitrate, are produced by TER and the AGR because of the high emissions of  $\text{NO}_2$  and  $\text{NH}_3$ . Second, POW and parts of IND are overhead sources. In the case of the same emissions, the impact of POW and the IND on the near-surface PM<sub>2.5</sub> concentration is less than that of the TRA, RES, and AGR. The contributions of the TRA, RES, and AGR are 3.0%, 7.2%, and 10.3%, respectively.

Fig. 6 shows the spatial distributions of the contributions to the

near-surface PM<sub>2.5</sub> from different sources. The distributions are significantly affected by the emission sources and meteorological conditions. During the research period, the dominant wind direction is northwest. Pollutant emissions affect the PM<sub>2.5</sub> concentration in the local and southeast areas. For LOC, the spatial distribution of the contribution is similar to that of the emission inventory (Fig. 1c). A high contribution is found in Tangshan urban area, which reaches 70%. LOC emission has significant impact on PM<sub>2.5</sub> concentration in Tangshan and surrounding regions. For IND, the high contribution region, reaching 45%, is also located in the Tangshan urban area. The PM<sub>2.5</sub> concentration in most parts of Tangshan is affected significantly by the IND emission. Based on the variance analysis, the impact of the POW, TRA, and RES emissions on the PM<sub>2.5</sub> concentration is not significant. The PM<sub>2.5</sub> concentration in the southeast of Tangshan is influenced significantly by the AGR emission, and the contribution reaches 14%.

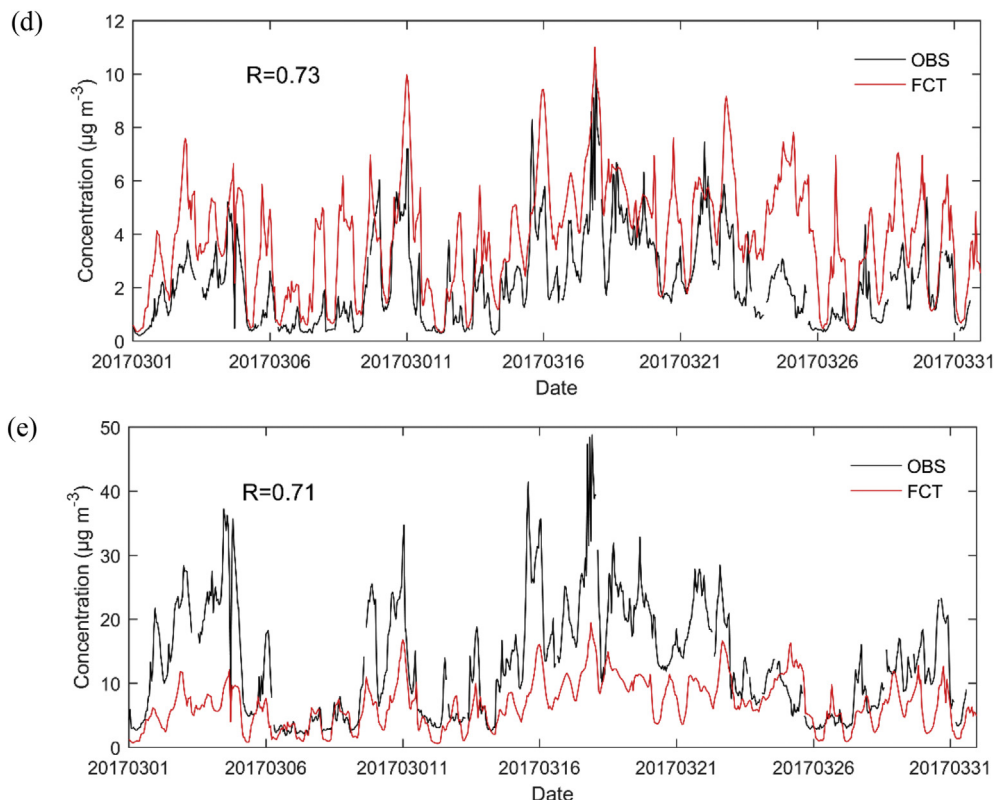


Fig. 4. (continued).

**Table 2**

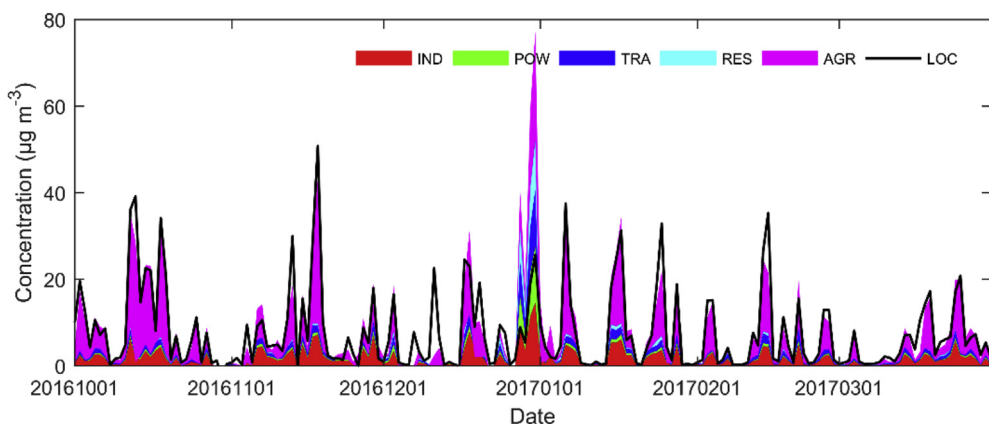
Statistical performances of the chemical components of  $\text{PM}_{2.5}$  during Mar. 2017 in Langfang.

	IOA	R	RMSE ( $\mu\text{g m}^{-3}$ )	MB ( $\mu\text{g m}^{-3}$ )	ME ( $\mu\text{g m}^{-3}$ )
$\text{SO}_4^{2-}$	0.44	0.72	21.6	-14.5	14.5
$\text{NH}_4^+$	0.83	0.70	5.3	-1.3	3.9
$\text{NO}_3^-$	0.58	0.55	21.5	9.6	12.4
OC	0.62	0.71	9.3	-2.2	7.0
EC	0.70	0.73	2.2	-6.5	1.8

**Table 3**

Contributions of emissions from the different sectors to the total emissions in Tangshan, as sourced from the MEIC (Unit: %).

	$\text{SO}_2$	$\text{NO}_2$	CO	$\text{PM}_{2.5}$	$\text{PM}_{10}$	$\text{NH}_3$
IND	87.0	64.9	79.4	88.0	88.8	7.2
POW	7.5	13.8	2.1	7.4	7.4	0.0
TRA	1.6	20.4	10.3	1.5	0.3	0.8
RES	4.0	0.8	8.2	3.1	3.4	1.7
AGR	0.0	0.0	0.0	0.0	0.0	90.3

Fig. 5. Daily contribution of IND, POW, TRA, RES, AGR, and LOC to the near-surface nitrate ( $\text{NO}_3^-$ ) concentration in Tangshan.

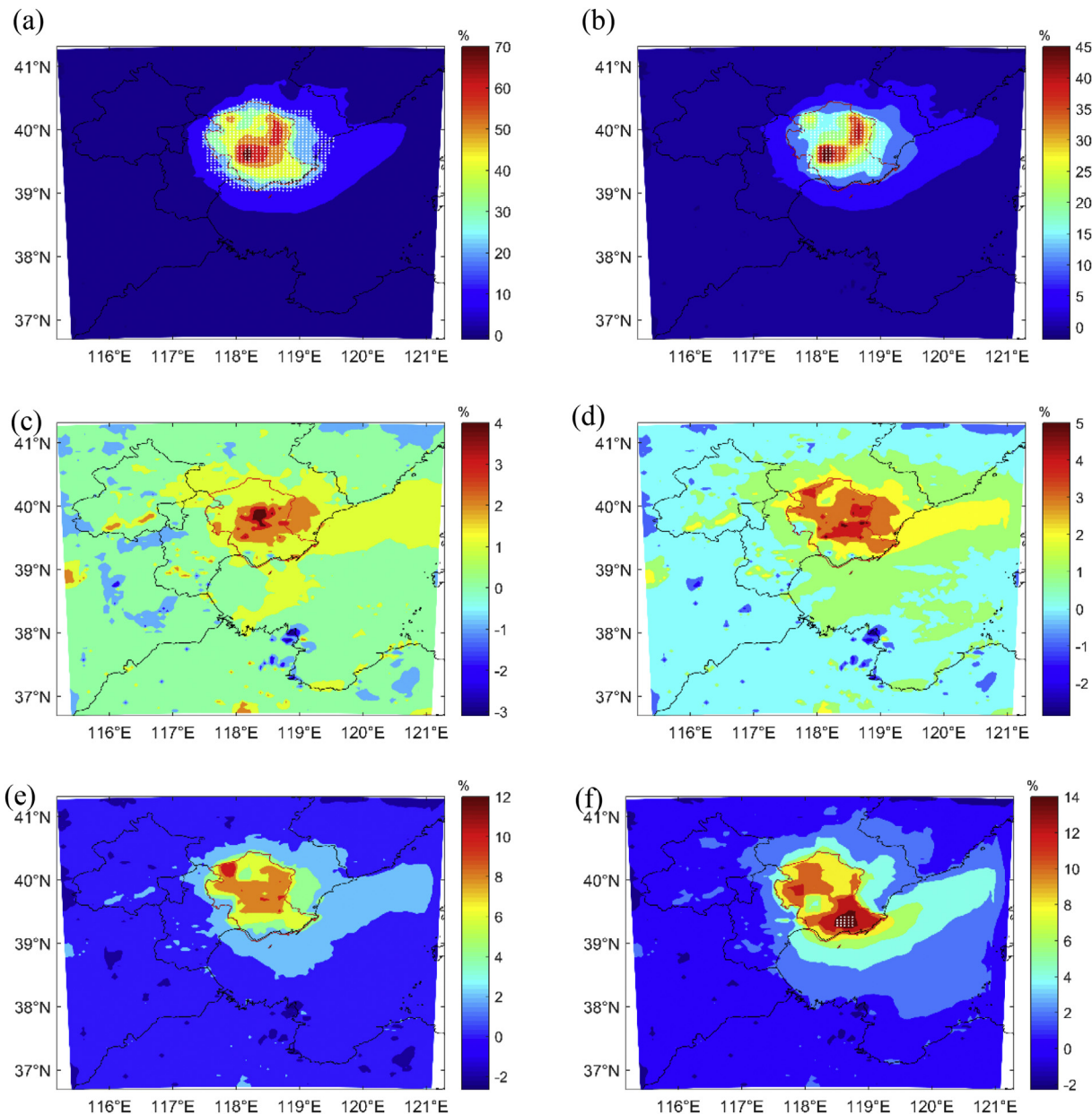


**Fig. 6.** Spatial distributions of the contributions of the LOC (a), IND (b), POW (c), TRA (d), RES (e), and AGR (f) emissions to the near-surface PM<sub>2.5</sub> mean concentration. The white points indicate that the change in the PM<sub>2.5</sub> concentration is significant between the BASE and SEN simulations, based on the variance analysis ( $p < 0.05$ ).

### 3.3. Impact of meteorological conditions on emission contribution

Meteorological conditions are key factors promoting daily changes in pollutant concentrations, and have significant influence on pollutant transport (He et al., 2017b; He et al., 2017c). This study investigates the impact of large-scale atmospheric circulation and local meteorological elements on the emission contribution. Fig. 7 shows the box plot of the daily mean contribution to the near-surface PM<sub>2.5</sub> for different circulation types. The local contribution is more remarkable for cold-air processes, and it is enhanced with the increase in the cold air intensity. For static weather, particularly for CT2, regional air pollution occurs, and the pollutant regional transport is notable, resulting in a low local contribution. Except for the AGR emission, the impact of the atmospheric circulation on contribution of local emissions from different sectors is similar to that of the total local emissions. The AGR emission

contributes secondary aerosols via the chemical processes of the conversion of ammonia to ammonium. The contribution of ammonium (Fig. 4) is positively correlated to the PM<sub>2.5</sub> concentration, with a correlation coefficient of 0.75. Previous studies have also revealed that the ratio of secondary aerosols is large in static weather or severe pollution processes (Huang et al., 2014). These results indicate that static weather is conducive to the formation of secondary aerosols, which can explain the high contribution of the AGR in static weather.

Table 4 lists the correlation between the contributions of the different emissions and local meteorological elements. T<sub>2</sub> and RH<sub>2</sub> (WS<sub>10</sub> and planetary boundary layer height (PBLH)) are negatively (positively) correlated to the contributions of the different emissions, except the AGR. This indicates that the conditions of high temperature and humidity, low wind speed, and PBLH are favourable for pollutant regional transport and decrease the impact of the

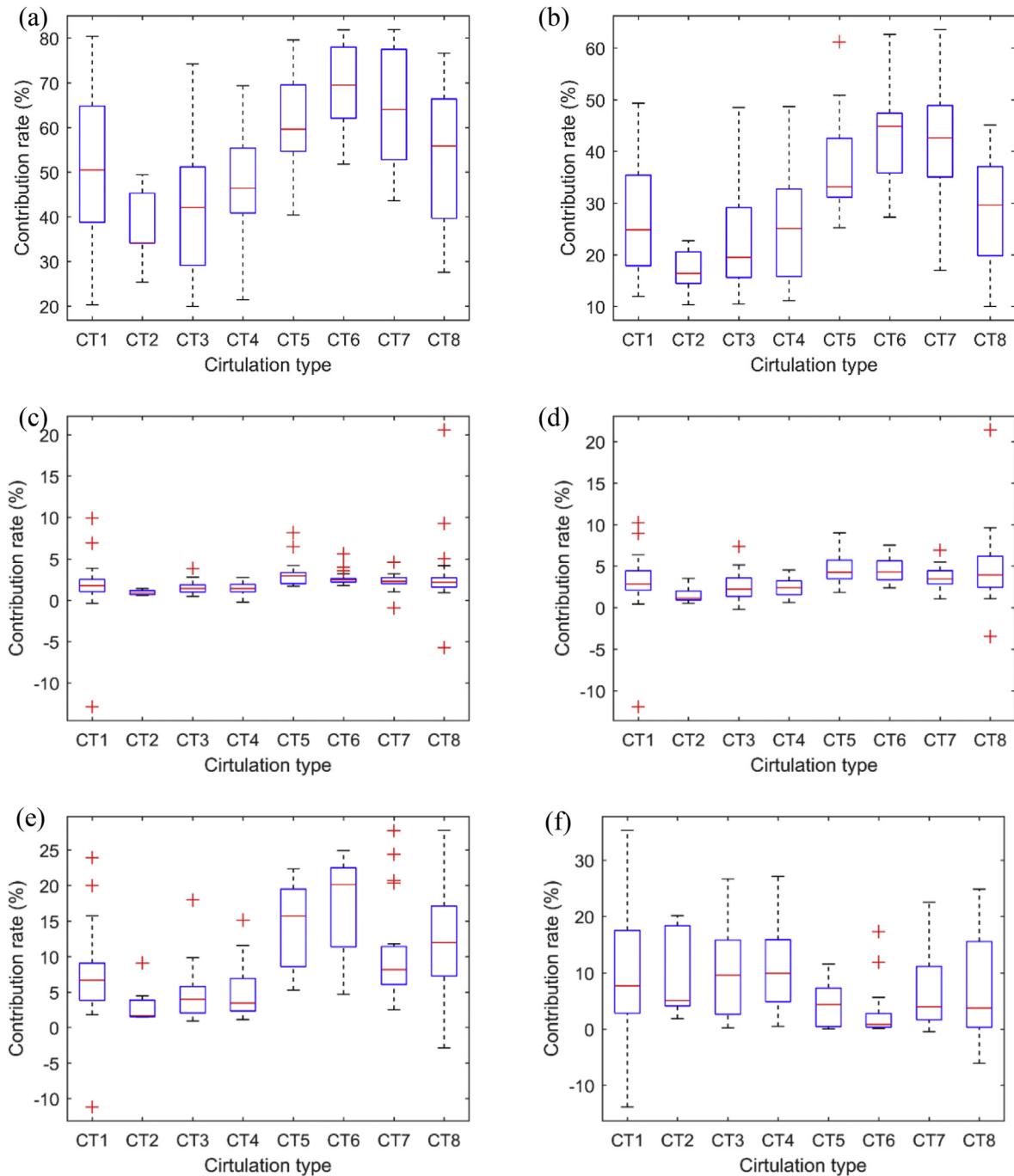


**Fig. 7.** Box plots of the daily mean contributions of the LOC (a), IND (b), POW (c), TRA (d), RES (e), and AGR (f) emissions to the near-surface PM<sub>2.5</sub> for the different circulation types. Red line, blue box, and black line represent the median, first and third quartiles, and maximum and minimum values, respectively. Data points beyond the whiskers are displayed using red plus. (For interpretation of the references to colour in this figure legend, the reader is referred to the Web version of this article.)

**Table 4**

Correlation coefficients between the contributions of the different emissions and local meteorological elements in Tangshan.

	LOC	IND	POW	TRA	RES	AGR
T <sub>2</sub>	-0.16*	-0.11	-0.25*	-0.32*	-0.67*	0.33*
RH <sub>2</sub>	-0.48*	-0.67*	-0.10	-0.16*	-0.52*	0.68*
WS <sub>10</sub>	0.02	0.21*	0.03	0.02	0.12	-0.28*
PBLH	0.38*	0.56*	-0.01	0.02	0.15*	-0.31*

\*Passes the significance test ( $p < 0.05$ ).

local emissions. The AGR contributes secondary aerosols to PM<sub>2.5</sub>. The environment of high temperature and humidity is favourable for gas-particle transformation, resulting in a positive correlation between the contributions of the AGR and T<sub>2</sub> and RH<sub>2</sub>. Generally, local meteorological conditions have significant effect on the source of PM<sub>2.5</sub>.

### 3.4. Backward trajectories and potential source regions

Except for the contributions of the different emission sources,

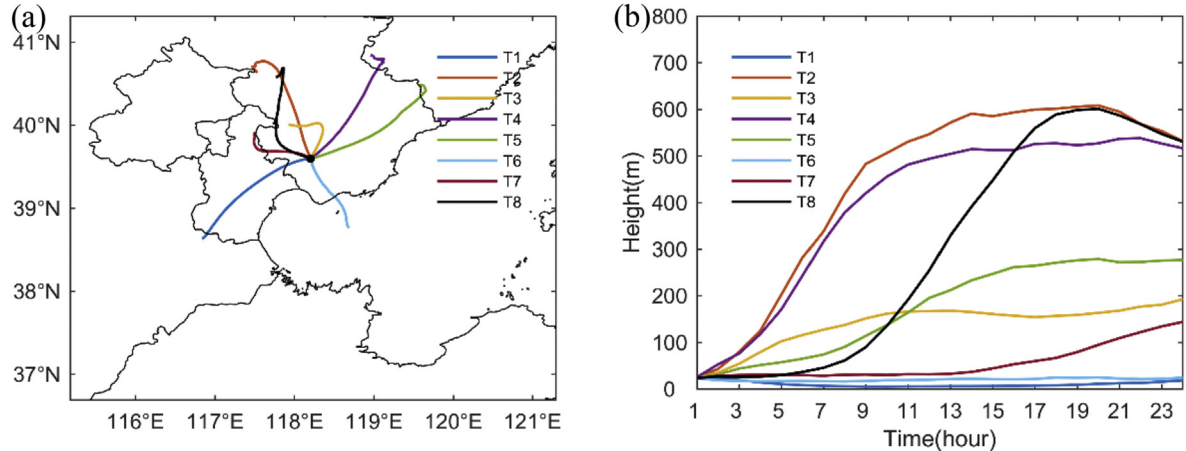


**Fig. 8.** Cluster-mean 24-h backward trajectories in horizontal (a) and vertical (b) directions. The receptor site (black point in Figure a) is located in the main urban area of Tangshan.

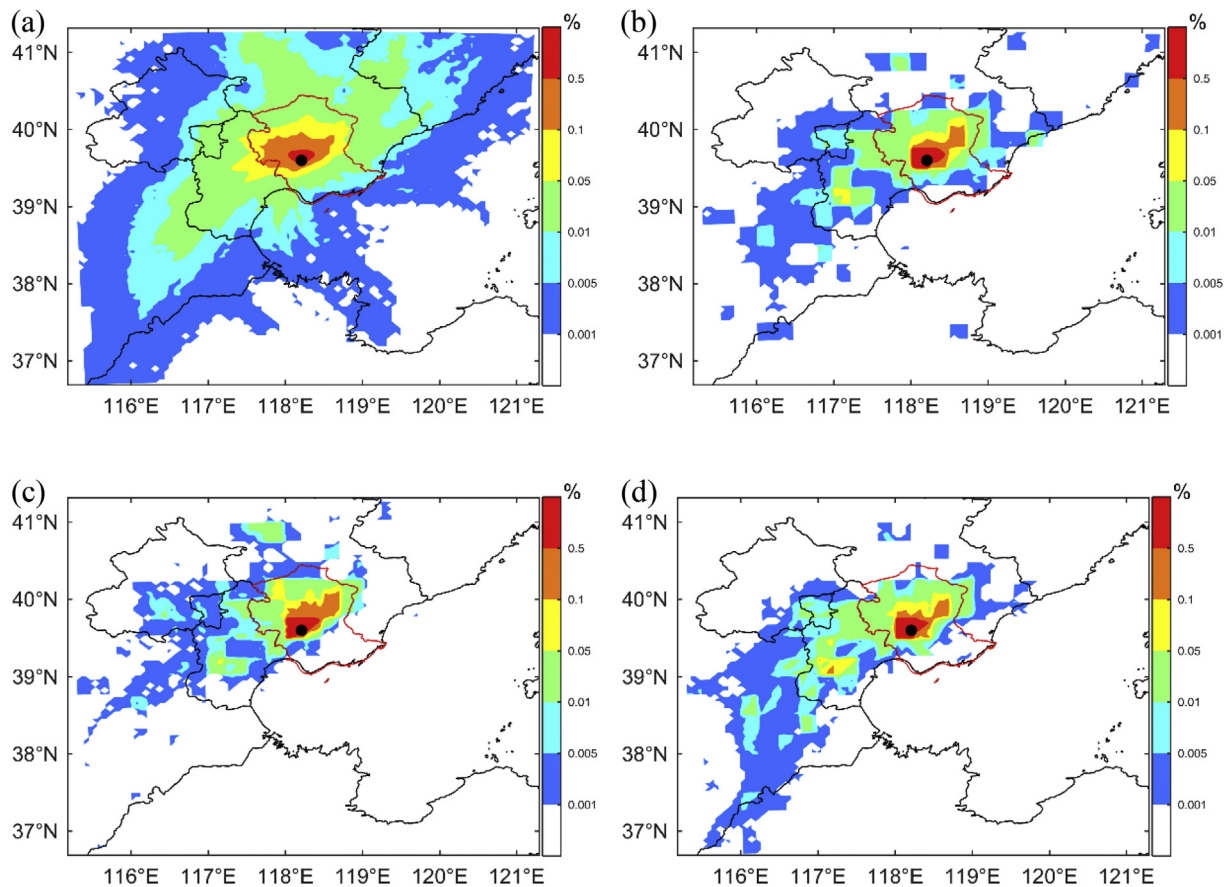


**Fig. 9.** Spatial distribution of the contribution of the air mass (a), PM<sub>2.5</sub> potential source regions (b), PM<sub>2.5</sub> potential source regions in cold air process (CT6, c), and PM<sub>2.5</sub> potential source regions in static weather (CT8, d). The black point represents the receptor point.

the spatial distribution of the contributions is extremely important for adopting measures to prevent and control air pollution. Backward trajectory is used frequently in the research on source analysis (He et al., 2017c; Liu et al., 2013). Based on the K-means cluster method, 8 cluster-mean 24-h backward trajectories for Tangshan are identified (Fig. 8). The ratios of the 8 cluster trajectories are 14.6% (T1), 9.7% (T2), 16.7% (T3), 9.9% (T4), 10.2% (T5), 9.1% (T6), 17.9% (T7), and 11.8% (T8). The average PM<sub>2.5</sub> concentrations of the 8 cluster trajectories are 105.1  $\mu\text{g m}^{-3}$  (T1), 74.8  $\mu\text{g m}^{-3}$  (T2),

92.8  $\mu\text{g m}^{-3}$  (T3), 108.5  $\mu\text{g m}^{-3}$  (T4), 121.2  $\mu\text{g m}^{-3}$  (T5), 96.3  $\mu\text{g m}^{-3}$  (T6), 116.1  $\mu\text{g m}^{-3}$  (T7), and 92.2  $\mu\text{g m}^{-3}$  (T8). A large number of emission sources are located in the northeast direction of the receptor site (Fig. 1c), and the height of the northeast air mass (T4 and T5) is relatively low. These result in a high PM<sub>2.5</sub> concentration at the receptor site for T4 and T5. For the southwest (T1) and west (T7) air masses below 150 m, PM<sub>2.5</sub> easily flows from Tianjin, resulting in a relatively high concentration in the receptor site. Because few emission sources are distributed in the southeast of the receptor

site, PM<sub>2.5</sub> concentration is relatively low under the southeast air mass (T6). However, the atmosphere is easily blocked because of the high terrain in the north of the receptor site (Fig. 1). T3 and T8 have remarkable direction changes from the west to the northeast and from the north to the west, respectively. These two cluster trajectories indicate the occurrence of a cold air process, and PM<sub>2.5</sub> concentration is relatively low because of the favourable diffusion conditions. T2 represents a strong cold air process, and the PM<sub>2.5</sub> concentration is the lowest here in the eight trajectories.

Based on the contribution of the air mass (Fig. 9a), the sources of air mass are mainly from the southwest, north, and east of Tangshan. Affected by the source of the air mass and distributions of the emission sources, PM<sub>2.5</sub> at the receptor point is mainly from the Tangshan local emissions, which is consistent with the results from the WRF-Chem sensitivity simulation, exhibiting a more than 70% contribution in the Tangshan urban area. Tianjin is another important potential source region for the receptor site. Surrounding cities, such as Qinhuangdao, Chengde, Langfang, and Baoding, are also potential source regions. In some areas where the cities or industrial regions are densely distributed, such as the Beijing–Tianjin–Hebei region in China, a joint control of the emissions can substantially improve the air quality. The atmospheric circulation has a significant effect on PM<sub>2.5</sub> potential source area (Fig. 9c and d). In cold air process, PM<sub>2.5</sub> mainly sources from the local emissions. While in static weather, Tianjin and the eastern part of Hebei have made important contributions to PM<sub>2.5</sub> in Tangshan.

#### 4. Conclusions

Air pollution problems have attracted the attention of the government and public of China. Understanding the sources of the pollutants is helpful in the prevention and control of air pollution. Using the WRF-Chem and WRF-FLEXPART models, this study analyses the contributions of the local emissions to the PM<sub>2.5</sub> concentration, backward trajectory, and potential source regions in Tangshan.

Generally, the WRF-Chem can well reproduce the spatial–temporal variations of the meteorological and pollutant concentration fields, which is the basis of the source apportionment research. Based on the emission switch on/off sensitivity simulations, the contribution of the total local emissions to the near-surface PM<sub>2.5</sub> concentration is 46.0% in Tangshan and more than 70% in the urban Tangshan areas. The contributions of the local industrial emissions, local power plant emissions, local traffic emissions, local resident emissions, and local agricultural emissions are 23.1, 2.0, 3.0, 7.2, and 10.3%, respectively. Based on the variance analysis, the impact of the total local emissions and local industrial emissions is significant in Tangshan, whereas it is significant for the agricultural emissions in the southeast of Tangshan. Large-scale circulation and local meteorological conditions have a significant effect on the source of PM<sub>2.5</sub>. Under static weather, the impact of the regional transport is enhanced. Eight backward trajectories are identified from the FLEXPART simulation. The PM<sub>2.5</sub> concentrations in receptor site (Tangshan) for eight backward trajectories have a major difference. The ratio of the west air mass is the highest in the eight trajectories. The northeast air mass results in serious air pollution because numerous emission sources are located in the northeast of Tangshan. The main potential source region of PM<sub>2.5</sub> is distributed in Tangshan and Tianjin.

Our results are extremely important for understanding the cause of air pollution and helpful in the prevention and control of air pollution in Tangshan. A joint control of emissions is strongly recommended and can substantially improve the air quality in some areas where cities or industrial regions are densely distributed. A comparison of the different source apportionment methods

should be performed in the future to decrease the uncertainty in the pollutant sources in Tangshan.

#### CRediT authorship contribution statement

**Jianjun He:** Writing - original draft, Writing - review & editing, Conceptualization, Methodology, Software, Investigation, Visualization. **Lei Zhang:** Writing - review & editing. **Zhanyu Yao:** Writing - review & editing. **Huizheng Che:** Supervision, Writing - review & editing. **Sunling Gong:** Supervision, Writing - review & editing. **Min Wang:** Software, Investigation, Visualization. **Mengxue Zhao:** Software, Investigation, Visualization. **Boyu Jing:** Writing - review & editing.

#### Declaration of competing interest

I declare on behalf of my co-authors that the work described is original research that has not been published previously, and not under consideration for publication elsewhere, in whole or in part. All the authors listed have approved the manuscript that is enclosed.

#### Acknowledgments

This work was supported by the National Natural Science Foundation of China (No. 91744209, 41975131, 41705080, 41775139), Key Project of Strategic International Scientific and Technological Innovation Cooperation of the Ministry of Science and Technology (No. 2016YFE0201900), the Opening Research Foundation of State Environmental Protection Key Laboratory of Odor Pollution Control, P.R. China (No. 201903102), and the CMA Innovation Team for Haze-fog Observation and Forecasts.

#### References

- An, X.Q., Tao, Y., Mi, S.Q., Sun, Z.B., Hou, Q., 2015. Association between PM<sub>10</sub> and respiratory hospital admissions in different seasons in heavily polluted Lanzhou city. *J. Environ. Health* 77, 64–71.
- Balzarini, A., Pirovano, G., Honzak, L., Zubkar, R., Curci, G., Forkel, R., Hirtl, M., San Jose, R., Tuccella, P., Grell, G.A., 2015. WRF-Chem model sensitivity to chemical mechanisms choice in reconstructing aerosol optical properties. *Atmos. Environ.* 115, 604–619.
- Brioude, J., Arnold, D., Stohl, A., Cassiani, M., Morton, D., Seibert, P., Angevine, W., Evan, S., Dingwell, A., Fast, J.D., Easter, R.C., Pisso, I., Burkhardt, J., Wotawa, G., 2013. The Lagrangian particle dispersion model FLEXPART-WRF version 3.1. *Geosci. Model Dev. (GMD)* 6, 1889–1904.
- Carvalho, D., Rocha, A., Gomez-Gesteira, M., Santos, C., 2012. A sensitivity study of the WRF model in wind simulation for an area of high wind energy. *Environ. Model. Software* 33, 23–34.
- Chai, F.H., Gao, J., Chen, Z.X., Wang, S.L., Zhang, Y.C., Zhang, J.Q., Zhang, H.F., Yun, Y.R., Ren, C., 2014. Spatial and temporal variation of particulate matter and gaseous pollutants in 26 cities in China. *J. Environ. Sci.* 26, 75–82.
- Chen, F., Dudhia, J., 2001. Coupling an advanced land surface-hydrology model with the Penn State-NCAR MM5 modeling system. Part I: Model implementation and sensitivity. *Mon. Weather Rev.* 129, 569–585.
- Chen, Y., Wild, O., Ryan, E., Sahu, S.K., Lowe, D., Archer-Nicholls, S., Wang, Y., McFiggans, G., Ansari, T., Singh, V., Sokhi, R.S., Archibald, A., Beig, G., 2020. Mitigation of PM<sub>2.5</sub> and ozone pollution in Delhi. A sensitivity study during the pre-monsoon period. *Atmos. Chem. Phys.* 20, 499–514.
- Clappier, A., Belis, C.A., Pernigotti, D., Thunis, P., 2017. Source apportionment and sensitivity analysis: Two methodologies with two different purposes. *Geosci. Model Dev. (GMD)* 10, 4245–4256.
- Ding, A.J., Wang, T., Fu, C.B., 2013. Transport characteristics and origins of carbon monoxide and ozone in Hong Kong, South China. *J. Geophys. Res. Atmos.* 118, 9475–9488.
- Dordević, D., Tosić, I., Šakan, S., Petrović, S., Duricic-Milanković, J., Finger, D.C., Dagsson-Waldhauserova, P., 2019. Can volcanic dust suspended from surface soil and deserts of Iceland be transferred to central Balkan similarly to African dust (Sahara)? *Front. Earth Sci.* 7, 12.
- Dudhia, J., 1989. Numerical study of convection observed during the winter monsoon experiment using a mesoscale two-dimensional model. *J. Atmos. Sci.* 46, 3077–3107.
- Dunker, A.M., Yarwood, G., Ortmann, J.P., Wilson, G.M., 2002. The decoupled direct method for sensitivity analysis in a three-dimensional air quality model –

- implementation, accuracy, and efficiency. *Environ. Sci. Technol.* 36, 2965–2976.
- Gao, M., Carmichael, G.R., Wang, Y.S., Ji, D.S., Liu, Z.R., Wang, Z.F., 2016. Improving simulations of sulfate aerosols during winter haze over Northern China: The impacts of heterogeneous oxidation by NO<sub>2</sub>. *Front. Environ. Sci. Eng.* 10, 11.
- Gao, Y., Liu, X., Zhao, C., Zhang, M., 2011. Emission controls versus meteorological conditions in determining aerosol concentrations in Beijing during the 2008 Olympic Games. *Atmos. Chem. Phys.* 11, 12437–12451.
- He, J.J., Gong, S.L., Liu, H.L., An, X.Q., Yu, Y., Zhao, S.P., Wu, L., Song, C.B., Zhou, C.H., Wang, J., Yin, C.M., Yu, L.J., 2017a. Influences of meteorological conditions on interannual variations of particulate matter pollution during winter in the Beijing-Tianjin-Hebei area. *J. Meteorol. Res.* 31, 1062–1069.
- He, J.J., Gong, S.L., Yu, Y., Yu, L.J., Wu, L., Mao, H.J., Song, C.B., Zhao, S.P., Liu, H.L., Li, X.Y., Li, R.P., 2017b. Air pollution characteristics and their relation to meteorological conditions during 2014–2015 in major Chinese cities. *Environ. Pollut.* 223, 484–496.
- He, J.J., Gong, S.L., Zhou, C.H., Lu, S.H., Wu, L., Chen, Y., Yu, Y., Zhao, S.P., Yu, L.J., Yin, C.M., 2018. Analyses of winter circulation types and their impacts on haze pollution in Beijing. *Atmos. Environ.* 192, 94–103.
- He, J.J., Mao, H.J., Gong, S.L., Yu, Y., Wu, L., Liu, H.L., Chen, Y., Jing, B.Y., Ren, P.P., Zou, C., 2017c. Investigation of particulate matter regional transport in Beijing based on numerical simulation. *Aerosol Air Quality Res.* 17, 1181–1189.
- He, J.J., Wu, L., Mao, H.J., Liu, H.L., Jing, B.Y., Yu, Y., Ren, P.P., Feng, C., Liu, X.H., 2016. Development of a vehicle emission inventory with high temporal-spatial resolution based on NRT traffic data and its impact on air pollution in Beijing - Part 2: Impact of vehicle emission on urban air quality. *Atmos. Chem. Phys.* 16, 3171–3184.
- He, J.J., Yu, L.J., Liu, N., Zhao, S.P., Chen, J.B., 2014. Impact of land surface information on WRF's performance in complex terrain area. *Chin. J. Atmos. Sci.* 38, 484–498.
- He, J.J., Yu, Y., Yu, L.J., Liu, N., Zhao, S.P., 2017d. Impacts of uncertainty in land surface information on simulated surface temperature and precipitation over China. *Int. J. Climatol.* 37, 829–847.
- Hong, S.-Y., Lim, J.-O.J., 2006. The WRF single-moment 6-class microphysics scheme (WSM6). *Asia-Pacific J. Atmos. Sci.* 42, 129–151.
- Hong, S.Y., Noh, Y., Dudhia, J., 2006. A new vertical diffusion package with an explicit treatment of entrainment processes. *Mon. Weather Rev.* 134, 2318–2341.
- Huang, R.J., Zhang, Y.L., Bozzetti, C., Ho, K.F., Cao, J.J., Han, Y.M., Daellenbach, K.R., Slowik, J.G., Platt, S.M., Canonaco, F., Zotter, P., Wolf, R., Pieber, S.M., Bruns, E.A., Crippa, M., Ciarelli, G., Piazzalunga, A., Schwikowski, M., Abbaszade, G., Schnelle-Kreis, J., Zimmermann, R., An, Z.S., Szidat, S., Baltensperger, U., El Haddad, I., Prevot, A.S.H., 2014. High secondary aerosol contribution to particulate pollution during haze events in China. *Nature* 514, 218–222.
- Kain, J.S., 2004. The Kain-Fritsch convective parameterization: An update. *J. Appl. Meteorol.* 43, 170–181.
- Koo, B., Wilson, G.M., Morris, R.E., Dunker, A.M., Yarwood, G., 2009. Comparison of source apportionment and sensitivity analysis in a particulate matter air quality model. *Environ. Sci. Technol.* 43, 6669–6675.
- Liu, N., Yu, Y., He, J.J., Zhao, S.P., 2013. Integrated modeling of urban-scale pollutant transport: Application in a semi-arid urban valley, Northwestern China. *Atmos. Pollut. Res.* 4, 306–314.
- Mlawer, E.J., Taubman, S.J., Brown, P.D., Iacono, M.J., Clough, S.A., 1997. Radiative transfer for inhomogeneous atmosphere: RRTM, a validated correlated-k model for the longwave. *J. Geophys. Res. Atmos.* 102, 16663–16682.
- Mulder, M.D., Dumanoglu, Y., Efstathiou, C., Kukucka, P., Matejovicova, J., Maurer, C., Pribylova, P., Prokes, R., Sofuoğlu, A., Sofuoğlu, S.C., Wilson, J., Zetzs, C., Wotawa, G., Lammel, G., 2019. Fast formation of Nitro-PAHs in the marine atmosphere constrained in a regional-scale Lagrangian field experiment. *Environ. Sci. Technol.* 53, 8914–8924.
- Saikawa, E., Kim, H., Zhong, M., Avramov, A., Zhao, Y., Janssens-Maenhout, G., Kurokawa, J., Klimont, Z., Wagner, F., Naik, V., Horowitz, L.W., Zhang, Q., 2017.
- Comparison of emissions inventories of anthropogenic air pollutants and greenhouse gases in China. *Atmos. Chem. Phys.* 17, 6393–6421.
- Schell, B., Ackermann, I.J., Hass, H., Binkowski, F.S., Ebel, A., 2001. Modeling the formation of secondary organic aerosol within a comprehensive air quality model system. *J. Geophys. Res. Atmos.* 106, 28275–28293.
- Shi, G.L., Liu, J.Y., Wang, H.T., Tian, Y.Z., Wen, J., Shi, X.R., Feng, Y.C., Ivey, C.E., Russell, A.G., 2018. Source apportionment for fine particulate matter in a Chinese city using an improved gas-constrained method and comparison with multiple receptor models. *Environ. Pollut.* 233, 1058–1067.
- Song, C.B., He, J.J., Wu, L., Jin, T.S., Chen, X., Li, R.P., Ren, P.P., Zhang, L., Mao, H.J., 2017a. Health burden attributable to ambient PM<sub>2.5</sub> in China. *Environ. Pollut.* 223, 575–586.
- Song, C.B., Wu, L., Xie, Y.C., He, J.J., Chen, X., Wang, T., Lin, Y.C., Jin, T.S., Wang, A.X., Liu, Y., Dai, Q.L., Liu, B.S., Wang, Y.N., Mao, H.J., 2017b. Air pollution in China: Status and spatiotemporal variations. *Environ. Pollut.* 227, 334–347.
- Stockwell, W.R., Middleton, P., Chang, J.S., Tang, X., 1990. The second generation regional acid deposition model chemical mechanism for regional air quality modeling. *J. Geophys. Res.* 95, 16343–16367.
- Thunis, P., Clappier, A., Tarrason, L., Cuvelier, C., Monteiro, A., Pisoni, E., Wesseling, J., Belisa, C.A., Pirovano, G., Janssen, S., Guerreiro, C., Peduzzi, E., 2019. Source apportionment to support air quality planning: Strengths and weaknesses of existing approaches. *Environ. Int.* 130, 13.
- Wang, F., Chen, D.S., Cheng, S.Y., Li, J.B., Li, M.J., Ren, Z.H., 2010. Identification of regional atmospheric PM10 transport pathways using HYSPLIT, MM5-CMAQ and synoptic pressure pattern analysis. *Environ. Model. Software* 25, 927–934.
- Wang, Y., Chen, Y., Wu, Z.J., Shang, D.J., Bian, Y.X., Du, Z.F., Schmitt, S.H., Su, R., Gkatzelis, G.I., Schlag, P., Hohaus, T., Voliotis, A., Lu, K.D., Zen, L.M., Zhao, C.S., Alfarra, M.R., McFiggans, G., Wiedensohler, A., Kiendler-Scharr, A., Zhang, Y.H., Hu, M., 2020. Mutual promotion between aerosol particle liquid water and particulate nitrate enhancement leads to severe nitrate-dominated particulate matter pollution and low visibility. *Atmos. Chem. Phys.* 20, 2161–2175.
- Wang, Z.S., Chien, C.J., Tonnesen, G.S., 2009. Development of a tagged species source apportionment algorithm to characterize three-dimensional transport and transformation of precursors and secondary pollutants. *J. Geophys. Res. Atmos.* 114, 17.
- Yang, Y., Liao, H., Lou, S., 2016. Increase in winter haze over eastern China in recent decades: Roles of variations in meteorological parameters and anthropogenic emissions. *J. Geophys. Res. Atmos.* 121, 13050–13065.
- Zhai, S.X., An, X.Q., Zhao, T.L., Sun, Z.B., Wang, W., Hou, Q., Guo, Z.Y., Wang, C., 2018. Detection of critical PM<sub>2.5</sub> emission sources and their contributions to a heavy haze episode in Beijing, China, using an adjoint model. *Atmos. Chem. Phys.* 18, 6241–6258.
- Zhang, J.Y., Zheng, M., Cai, J., Yan, C.Q., Hu, Y.T., Russell, A.G., Wang, X.S., Wang, S.X., Zhang, Y.H., 2015a. Comparison and overview of PM<sub>2.5</sub> source apportionment methods (in Chinese) *Chinese Science Bulletin* 60, 109–121.
- Zhang, L., Liu, L.C., Zhao, Y.H., Gong, S.L., Zhang, X.Y., Henze, D.K., Capps, S.L., Fu, T.M., Zhang, Q., Wang, Y.X., 2015b. Source attribution of particulate matter pollution over North China with the adjoint method. *Environ. Res. Lett.* 10, 8.
- Zhang, Z.Y., Xu, X.D., Qiao, L., Gong, D.Y., Kim, S.J., Wang, Y.J., Mao, R., 2018. Numerical simulations of the effects of regional topography on haze pollution in Beijing. *Sci. Rep.* 8, 11.
- Zhao, S.P., Yu, Y., Yin, D.Y., He, J.J., Liu, N., Qu, J.J., Xiao, J.H., 2016. Annual and diurnal variations of gaseous and particulate pollutants in 31 provincial capital cities based on in situ air quality monitoring data from China National Environmental Monitoring Center. *Environ. Int.* 86, 92–106.
- Zheng, B., Zhang, Q., Zhang, Y., He, K.B., Wang, K., Zheng, G.J., Duan, F.K., Ma, Y.L., Kimoto, T., 2015. Heterogeneous chemistry: a mechanism missing in current models to explain secondary inorganic aerosol formation during the January 2013 haze episode in North China. *Atmos. Chem. Phys.* 15, 2031–2049.